

Measuring Cosmological Distances Using Cluster Edges as a Standard Ruler

Erika L. Wagoner,^{1*} Eduardo Rozo,¹ Han Aung,² Daisuke Nagai^{2,3}

¹*Department of Physics, University of Arizona, 1118 E. Fourth Street, Tucson, AZ, 85721, USA*

²*Department of Physics, Yale University, New Haven, CT 06520, USA*

³*Department of Astronomy, Yale University, New Haven, CT 06520, USA*

Accepted XXX. Received YYY; in original form ZZZ

ABSTRACT

The line-of-sight velocity dispersion profile of galaxy clusters exhibits a “kink” corresponding to the spatial extent of orbiting galaxies. Because the spatial extent of a cluster is correlated with the amplitude of the velocity dispersion profile, we can utilise this feature as a gravity-calibrated standard ruler. Specifically, the amplitude of the velocity dispersion data allows us to infer the physical cluster size. Consequently, observations of the angular scale of the “kink” in the profile can be translated into a distance measurement to the cluster. Assuming the relation between cluster radius and cluster velocity dispersion can be calibrated from simulations, we forecast that with existing data from the Sloan Digital Sky Survey (SDSS) we will be able to measure the Hubble constant with 3.0% precision. Implementing our method with data from the Dark Energy Spectroscopic Instrument (DESI) will result in a 1.3% measurement of the Hubble constant. Adding cosmological supernova data improves the uncertainty of the DESI measurement to 0.7%.

Key words: methods: data analysis – galaxies: clusters: general – distance scale

1 INTRODUCTION

One of the greatest challenges to the standard model of modern cosmology is the 4.4σ tension between the Hubble constant (H_0) inferred from the Cosmic Microwave Background (CMB; Planck Collaboration et al. 2018) and that from supernova measurements by the SH0ES team (Riess et al. 2019). This discrepancy could be the first hint of a breakdown of the standard model of cosmology, and has therefore led to a broad range of new theoretical ideas for how this tension can be resolved (for a very nice review see Knox & Millea 2020). To unambiguously establish the need for new physics, an independent confirmation of the Hubble tension must be achieved.

Despite tremendous progress in this regard (for a discussion of recent results see e.g. Verde et al. 2019), the picture is not yet clear: while the predicted value for the Hubble constant from early-universe physics is quite robustly predicted, the local value of the Hubble constant is less robustly determined. Specifically, an independent distance ladder calibration of the Hubble constant using the tip of the red giant branch method results in a lower Hubble constant value ($h = 0.696 \pm 0.019$, Freedman et al. 2020). Distance calibrations via surface brightness fluctuations results in an intermediate Hubble value, consistent with the SH0ES and early-universe estimates ($h = 0.705 \pm 0.034$, Khetan et al. 2020), while cosmic chronometers also favour low Hubble values (e.g. Haridasu et al. 2018; Gómez-Valent & Amendola 2019). Early strong lensing constraints from the HOLICOW team favoured a high Hubble value ($h = 0.733 \pm 0.017$, Wong et al. 2020), but these values are sensitive to the detailed radial profile assumed for the lenses (Kochanek 2020). Allowing for

greater freedom in the mass models for the lenses while incorporating galaxy velocity dispersion data results in a low Hubble constant estimate ($h = 0.674 \pm 0.04$, Birrer et al. 2020). On the other hand, megamaser-based geometric distances lead to a high H_0 value ($h = 0.74 \pm 0.03$, Pesce et al. 2020). While gravitational waves may soon be able to resolve this dichotomy, current constraints are still limited by low number statistics (The LIGO Scientific Collaboration & the Virgo Collaboration 2019). Additional discussion can be found in Di Valentino et al. (2020).

In light of the current state of affairs, any new independent distance estimator is of great interest, provided the measurement can achieve percent level precision. In this paper, we propose one such method. Our method makes use of the cluster edge radius identified by Tomooka et al. (2020; hereafter Paper I) and the corresponding dark matter halo edge radius identified by Aung et al. (2020; hereafter Paper II). These radii appear to be intimately related to (but are somewhat larger than) the more well known splashback radius (see e.g. Bertschinger 1985; Adhikari et al. 2014; More et al. 2015; Diemer 2020). While the splashback radius of galaxy clusters can also be inferred from the galaxy distribution of the clusters (e.g. More et al. 2016; Chang et al. 2018; Zürcher & More 2019; Shin et al. 2019; Murata et al. 2020) and through weak lensing (Umetsu & Diemer 2017; Contigiani et al. 2019), this radial feature is much less pronounced than the edge radius identified in Paper I. In addition, splashback detection via galaxy distributions is known to be sensitive to selection effects (Busch & White 2017; Sunayama & More 2019). A similar bias may take place when measuring edge radii with velocity dispersions, though one benefits from the fact that cluster selection is done based on the galaxy density and not the velocity dispersion itself. Consequently, we expect such biases to be reduced.

* E-mail: wagoner47@email.arizona.edu (ELW)

Here, we treat the cluster edge radius in the velocity dispersion as a standard ruler which can be calibrated in simulations. Combined with the model of the phase space structure of clusters presented in [Paper I](#), we show that we are able to measure the angular diameter distance using the relative line-of-sight velocities of galaxies around clusters. The structure of this paper is as follows. We describe our method in section 2. In section 3 we demonstrate our method on current data and in section 4, and predict how our method will perform with near-future data. Our conclusions are presented in section 5. Throughout the paper, unless otherwise stated, we assume a fiducial Flat Λ CDM cosmology with $h = 0.7$ and $\Omega_m = 0.3$. We emphasise that this paper is *not* presenting a new measurement of the Hubble constant. Rather, our goal is simply to determine whether the method proposed here is sufficiently interesting to merit further investigation.

2 METHODOLOGY

2.1 The Key Idea

Fig. 1, taken directly from [Paper I](#), shows the radial profile of the stacked line-of-sight velocity dispersion of galaxies relative to the central galaxy of SDSS redMaPPer clusters. The points with error bars are the SDSS measurements, while the blue band corresponds to the best fit model of [Paper I](#). The key feature we would like to highlight is the obvious “kink” on this plot. This kink was interpreted in [Paper I](#) as the spatial extent of galaxies orbiting redMaPPer clusters, and we referred to this scale as the edge radius. This interpretation received theoretical support from [Paper II](#), which analysed the three dimensional analysis of substructure velocities around dark matter halos in a numerical simulation, and established the presence of a qualitatively similar feature in the three-dimensional velocity field. They also demonstrated that this edge radius is a simple re-scaling of the traditional splashback radius. In upcoming work, we will establish that the three dimensional “edge radius” observed in [Paper II](#) does in fact exactly corresponds to the “kink” in the line-of-sight velocity dispersion profile shown in fig. 1 ([Aung et al, in preparation](#)).

Our idea then is simple: it is relatively obvious that halos with larger line-of-sight velocity dispersions must also have larger edge radii. In other words, more massive halos occupy more space. We assume that we can use numerical simulations to calibrate a scaling relation between the velocity dispersion and edge radius of a halo, $R_{\text{edge}} = A\sigma_v^\alpha$. Using spectroscopic data, we can empirically measure σ_v^2 , which in turn determines the halo edge. At the same time, the same spectroscopic observations used to determine σ_v allow us to measure the velocity dispersion profile as a function of angular separation θ , thereby determining the angular scale θ_{kink} corresponding to the “kink” feature in fig. 1. The distance to a galaxy clusters is then recovered via

$$D_A(z_{\text{cluster}}) = \frac{R_{\text{edge}}}{\theta_{\text{kink}}} = \frac{A\sigma_v^\alpha}{\theta_{\text{kink}}} \quad (1)$$

where D_A is the angular diameter distance, and A and α are to be calibrated from simulations. With measurements of $D_A(z)$ at a variety of redshifts we can readily recover the Hubble parameter h .

In practice, things are a little more complicated: clusters do not have a single velocity dispersion: orbiting and infalling galaxies are kinematically distinct, and the line-of-sight velocity dispersion of both components varies with radius. Moreover, one must stack the signals of many clusters to achieve a high signal-to-noise measurement. However, one can readily accommodate these additional difficulties using forward-modelling as detailed below.

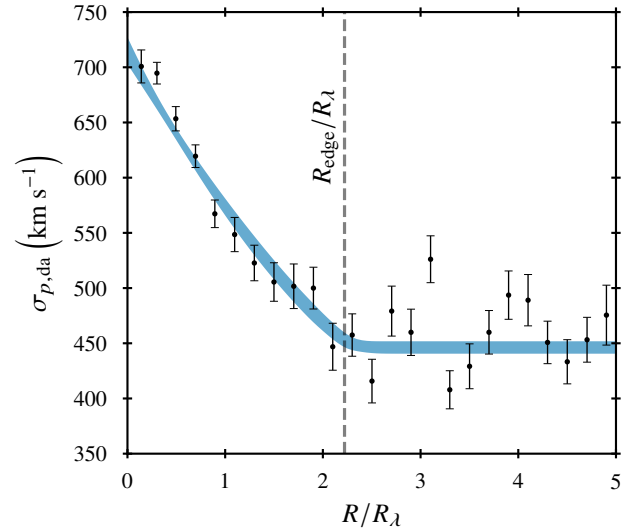


Figure 1. The radial dependence of the velocity dispersion of galaxies dynamically associated with SDSS redMaPPer clusters. At small radii, the velocity dispersion decreases with increasing radius. At large radii, the velocity dispersion appears constant with radius. The boundary between these two regimes is the cluster “edge radius” which we seek to use as a standard ruler. Recreated from the right panel of Figure 2 of [Paper I](#).

2.2 Full Forward Model

Following [Paper I](#) (albeit with slightly updated notation), we assume that the radial dependence of the line-of-sight velocity dispersion of orbiting galaxies in a cluster is given by

$$\sigma_{v,\text{orb}}(R) = \frac{\sigma_{\text{orb}}}{\sqrt{1 + kR/R_{\text{edge}}}}. \quad (2)$$

In the above equation, k is a shape parameter, which could be fit from the data, or which could be calibrated from numerical simulations. Here, we will conservatively assume that this shape parameter is fit from data rather than known a priori, but we will discuss the impact of such prior information throughout. The amplitude of the velocity dispersion profile for orbiting galaxies is governed by the parameter σ_{orb} . We assume in turn that this parameter is related to the halo edge radius via a simple power-law,

$$R_{\text{edge}} = R_p \left(\frac{\sigma_{\text{orb}}}{\bar{\sigma}_{\text{orb}}} \right)^a \left(\frac{1 + z_{\text{cen}}}{1 + z_p} \right)^b, \quad (3)$$

where $\bar{\sigma}_{\text{orb}}$ is a pivot scale set by the experimenter. Based on the results from [Paper I](#), we chose $\bar{\sigma}_{\text{orb}} = 788 \text{ km s}^{-1}$. Note that we have included a possible redshift dependence in the relation between velocity dispersion and edge radius. We assume the parameters R_p , a , and b are calibrated from simulation. These parameters could in principle be cosmology-dependent. Our naive expectation is that any such dependence will be weak, as the dynamical structure of the halo should primarily reflect the halo’s absolute mass. In practice, however, a dedicated calibration effort is clearly needed. For this work, our fiducial results will assume that R_p , a , and b are known, though we also consider how our results degrade as the uncertainty in these parameters increases. With these assumptions, the velocity dispersion profile of galaxy clusters is governed by either one or two parameters (σ_{orb} , k), depending on whether we assume the shape of the profile is fixed a priori or not.

When fitting survey data we are unable to fit each cluster individually. Instead, we consider a stack of galaxy clusters binned according to some mass proxy, e.g. the richness λ of redMaPPer clusters (though a similar analysis can be carried out for clusters stacked based on X-ray or SZ mass proxies). Here, we will assume the velocity dispersion of orbiting galaxies in a galaxy cluster is perfectly correlated with cluster richness, so that we can write

$$\sigma_{\text{orb}}(\lambda) = \sigma_{\text{p,orb}} \left(\frac{\lambda}{\lambda_{\text{p}}} \right)^{\alpha_{\text{orb}}} \left(\frac{1+z}{1+z_{\text{p}}} \right)^{\beta_{\text{orb}}} \quad (4)$$

Of course, in practice there will necessarily be scatter between the two mass tracers. Since our goal is to determine whether this type of analysis can in principle reach high precision, we will postpone the investigation of how scatter impacts our analyses to future work.

To summarise: eqn. (4) characterises the amplitude of the orbiting velocity dispersion profile as a function of richness. The edge radius of a cluster is a function of this orbiting velocity dispersion, and is given by eqn. (3). The radial dependence of the velocity dispersion profile is given by eqn. (2), where the shape parameter k can either be fit by the data or calibrated using numerical simulations. With this model in hand, the probability that an orbiting galaxy observed at a separation angle θ from the central galaxy of a cluster have line-of-sight velocity v is given by a Gaussian of zero mean and velocity dispersion $\sigma_{v,\text{orb}}(R)$ with $R = D_A \theta$.

The parameters so far only take into account the orbiting galaxies, while in fact, infalling and background galaxies must also be accounted for in the model. The velocity probability distribution for each of these components are also modelled as Gaussians with radius-independent velocity dispersions. The velocity dispersions are assumed to scale with richness and redshift, leading to analogues of eqn. (4):

$$\sigma_{\text{inf}}(\lambda) = \sigma_{\text{p,inf}} \left(\frac{\lambda}{\lambda_{\text{p}}} \right)^{\alpha_{\text{inf}}} \left(\frac{1+z}{1+z_{\text{p}}} \right)^{\beta_{\text{inf}}} \quad (5)$$

$$\sigma_{\text{los}}(\lambda) = \sigma_{\text{p,los}} \left(\frac{\lambda}{\lambda_{\text{p}}} \right)^{\alpha_{\text{los}}} \left(\frac{1+z}{1+z_{\text{p}}} \right)^{\beta_{\text{los}}} \quad (6)$$

The above consideration adds 6 parameters to our model, namely $\sigma_{\text{p,inf}}$ and $\sigma_{\text{p,los}}$, along with the corresponding richness and redshift slopes.

Finally, we must also model the radial profile of the fraction of galaxies that are orbiting, in-falling, and line-of-sight projections, all as a function of radius. The fraction of galaxies that are dynamically associated with the cluster (infalling or orbiting) is set to

$$f_{\text{da}}(R) = \begin{cases} 1 + a_1 (R/R_{\text{edge}}) & \text{for } R \leq R_{\text{edge}} \\ 1 + a_1 + b_1 (R/R_{\text{edge}} - 1) & \text{for } R \geq R_{\text{edge}} \end{cases} \quad (7)$$

This model differs from equation 14 of Paper I in that we do not include the quadratic term $a_2 (R/R_{\text{edge}})^2$ as a_2 was found to be consistent with zero. We also explicitly make the substitution $b_0 = 1 + a_1$ required for continuity at $R = R_{\text{edge}}$. The fraction of dynamically associated galaxies that are orbiting is set to

$$f_{\text{orb}}(R) = \begin{cases} c_0 + c_1 (R/R_{\text{edge}}) + c_2 (R/R_{\text{edge}})^2 & \text{for } R \leq R_{\text{edge}} \\ 0 & \text{for } R \geq R_{\text{edge}} \end{cases}, \quad (8)$$

where we enforce that the equation is continuous at R_{edge} by requiring that $c_0 = -(c_1 + c_2)$. These two radial profiles add an additional 4 free parameters (a_1 , b_1 , c_1 , and c_2) that are to be fit from the data, bringing the total number of free parameters in the model to 15. Our

final model for the line-of-sight velocity for a galaxy at an angular separation θ from a galaxy cluster of richness λ is

$$P(v, \theta) = f_{\text{da}} [f_{\text{orb}} G_{\text{orb}}(v) + (1 - f_{\text{orb}}) G_{\text{inf}}(v)] + (1 - f_{\text{da}}) G_{\text{los}}(v), \quad (9)$$

where G_{orb} , G_{inf} , and G_{los} are Gaussians with velocity dispersions $\sigma_{\text{orb}}(D_A \theta | \lambda)$, $\sigma_{\text{inf}}(\lambda)$ and $\sigma_{\text{los}}(\lambda)$, respectively. By fitting this model to spectroscopic survey data, we are able to measure the Hubble parameter h .

3 PROSPECTS FOR MEASURING H WITH SDSS

To estimate the constraining power of this cluster and galaxy sample, we begin by assuming the parameters linking the orbiting velocity dispersion to the edge radius are perfectly calibrated. Based on the results of Paper I, we set them to the values $R_{\text{p}} = 2.4$ Mpc, $a = 0.64$, and $b = -0.94$. Note that Paper I assumed a fixed cosmology to recover these parameters, so our analysis is circular. That is, we are *not* deriving any cosmological constraints. We are simply determining the precision with which we could measure h if the parameters R_{p} , a , and b were known from simulations.

We fit our model by sampling our 15-dimensional parameter space with a Markov Chain Monte Carlo (MCMC) via emcee¹ (Foreman-Mackey et al. 2013). We find $\sigma_h \approx 0.021$, corresponding to a 3% measurement of the Hubble constant. Note that our forecast of $\sigma_h \approx 0.021$ for an SDSS measurement is obtained while floating all 15 parameters in our model. In principle, numerical simulations could also fix or place priors on the parameters a_1 , b_1 , c_1 , c_2 , σ_{inf} , α_{inf} , and β_{inf} . When fixing these parameters in addition to k , we find $\sigma_h \approx 0.0088$, i.e. a 1.2% measurement of the Hubble constant with SDSS spectroscopy. We adopt the model in which all 15 parameters are allowed to float as our fiducial model, and use this as our basis for the DESI forecast.

In practice, our analysis will be sensitive to theoretical uncertainty in the input parameters R_{p} , a , and b linking the velocity dispersion to the cluster edge radius. To quantify the sensitivity of our measurement to this uncertainty, we repeat our measurement allowing for uncertainty in our calibration parameters. Specifically, we modify eqn. (3) by introducing three new parameters, Δ_{p} , Δ_a , and Δ_b , as per eqn. (10).

$$R_{\text{edge}} = R_{\text{p}} (1 + \Delta_{\text{p}}) \left(\frac{\sigma_{\text{orb}}(\lambda, z)}{\bar{\sigma}_{\text{orb}}} \right)^{a + \Delta_a} \left(\frac{1 + z_{\text{cen}}}{1 + z_{\text{p}}} \right)^{b + \Delta_b}. \quad (10)$$

We consider varying each of these new parameters, one at a time, while holding the other two fixed. When varying the calibration parameters Δ , we adopt a Gaussian prior for the parameter being varied. The prior has mean zero, with the standard deviation in Δ varied over the range 0.001 to 0.1. That is, the parameters Δ characterise the uncertainty with which the parameters R_{p} , a , and b are known. We find that the posterior in h is not sensitive to variations of these magnitudes in a or b . For the pivot radius R_{p} , however, we do see that σ_h increases with increasing calibration uncertainty as shown in fig. 2. The black dashed line in fig. 2 is the fiducial uncertainty, and the blue points are the recovered uncertainty when allowing Δ_{p} to vary. The orange line is our naive expectation due to error propagation,

$$\sigma_h = \sqrt{\left(\frac{h_{\text{fid}} \sigma_{R_{\text{p}}}}{R_{\text{p}}} \right)^2 + \sigma_{h,\text{fid}}^2}. \quad (11)$$

¹ <https://emcee.readthedocs.io/en/stable/>

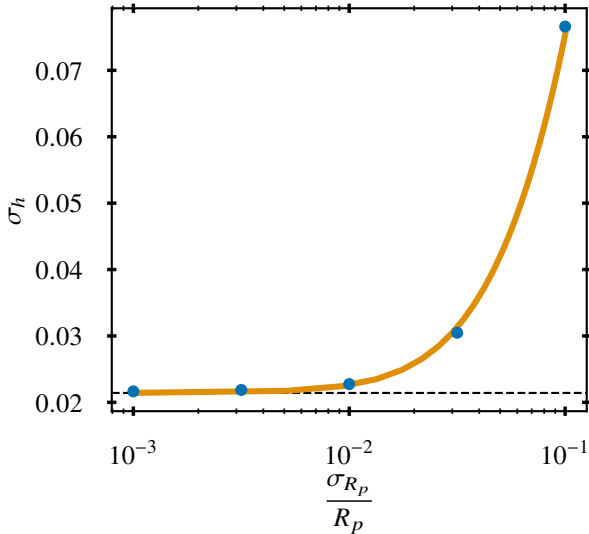


Figure 2. The uncertainty in h as a function of the uncertainty in the calibration of the pivot radius (blue points). The orange line is the naive expectation from error propagation (see eqn. (11)). The black dashed line is the fiducial estimate in the case of a perfect calibration.

Unsurprisingly, the quality of the recovered Hubble constant constraint is sensitive to uncertainties in the calibration of the relation between the halo edge and the halo velocity dispersion. In other words, enabling a percent level calibration of the Hubble constant using halo edges requires that halo edges be calibrated with better than percent level accuracy.

4 DESI FORECAST

In our SDSS forecast, we only considered variations in the Hubble parameter h in our analysis of SDSS data. By contrast, the DESI analysis will both reach higher precision and extend to higher redshifts, which will render the measurement sensitive to additional cosmological parameters. To determine the constraining power of our method in this case, we note that our measurement is intrinsically sensitive to D_A , which is itself proportional to h^{-1} . Consequently, we simply forecast the percent error for h in DESI with all other cosmological parameters fixed for a narrow redshift bin, and then reinterpret this error as a percent uncertainty in D_A . By doing this across a grid of redshifts, we arrive at an array of predicted constraints on D_A along this grid. The resulting Hubble diagram can then be fit to recover the cosmological parameters of interest.

Our DESI forecast assumes that the redMaPPer cluster catalogue is extended to redshift $z = 1$ across the full footprint. This is a best case scenario, but as we show below, it ends up helping with the interpretation of our results. The cluster density out to redshift 1 is estimated using the Dark Energy Survey (DES) Year 1 redMaPPer catalogue (McClintock et al. 2019). Specifically, we fit a power law to the number of redMaPPer clusters at low redshifts, and use this power law to estimate the number density at larger redshifts. We also estimate the galaxy density that is expected for the DESI survey from Figures 3.2 and 3.8 of DESI Collaboration et al. (2016). We use the estimated density of the Bright Galaxy Sample (BGS) for redshifts $z \in [0.1, 0.4)$. At redshifts $z \geq 0.4$, we use the average of the estimates from COSMOS (Ilbert et al. 2009) and SDSS for the

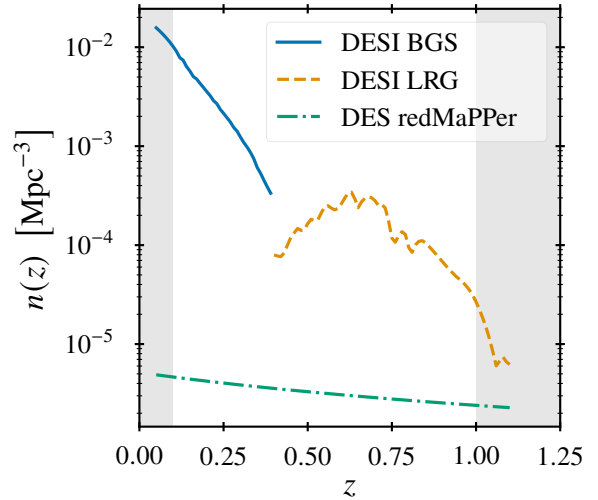


Figure 3. The number densities as a function of redshift used for the DESI BGS (blue solid line), DESI LRG (orange dashed line), and DES redMaPPer cluster (green dash-dotted line) samples. These number densities are used for the forecast, as described in section 4. Note that the DES number density is obtained by fitting a power law to the number of clusters as a function of redshift at lower redshifts, and then extending that power law to higher redshifts.

Luminous Red Galaxy (LRG) sample. The number density for both DESI galaxy samples as well as the cluster number density can be seen in fig. 3.

In the absence of systematics, we expect that the measured error on h will scale with the square-root of the number of galaxies used to estimate it, which we call N_m , where the subscript m indicates that these spectroscopic galaxies must be matched to a cluster. The expected uncertainty in h from a single redshift bin measurement, and assuming all other cosmological parameters are fixed, is given by

$$\sigma_h^{\text{DESI}}(z) = \sqrt{\frac{N_m^{\text{SDSS}}}{N_m^{\text{DESI}}(z)}} \sigma_h^{\text{SDSS}}, \quad (12)$$

where N_m^x is the number of matched galaxies found for survey x (SDSS or DESI). $\sigma_h^{\text{SDSS}} = 0.021$ is the measured error on h in SDSS as estimated in the previous section. The number of galaxies matched to a cluster in a redshift bin should be proportional to the number of clusters in that redshift bin times the average number of galaxies per cluster:

$$N_m(z) = C N_{\text{cl}}(z) N_{g/\text{cl}}(z), \quad (13)$$

where C is a proportionality constant.

The first term in eqn. (13) can be found as the number density of clusters times the volume within the redshift bin:

$$N_{\text{cl}}(z) = n_{\text{cl}}(z) V(z). \quad (14)$$

The second term in eqn. (13) is the number density of galaxies times the volume within which a galaxy is considered a match to the cluster, V_m :

$$N_{g/\text{cl}}(z) = n_g(z) V_m(z). \quad (15)$$

For the match volume, we consider the same criteria as in Paper I (section 3.1), assuming all clusters have a richness equal to the

median richness of the redMaPPer clusters. Our matching volume takes the form

$$V_m(z) = \frac{25\pi}{h^2} \left(\frac{\lambda(z)}{100} \right)^{0.4} [\chi(z + \Delta z) - \chi(z - \Delta z)] \quad (16)$$

where $2\Delta z$ is the width of the redshift bin of interest. The richness $\lambda(z)$ should in principle be the median richness within the redshift bin. In practice, however, the median richness of redMaPPer clusters was found to be largely independent of redshift, so for simplicity we used the median richness of all clusters when estimating the matching volume.

We determine the proportionality constant C in eqn. (13) using the SDSS data set. With these assumptions in hand, we can estimate the error σ_h inferred from clusters in redshift bins of width $\pm\Delta z = 0.05$ between $z = 0.1$ and $z = 1$. As noted earlier, in practice, our measurement is sensitive to D_A , not h , so we re-interpret the predicted error in h as a percent error on D_A at a grid of redshifts $z = 0.15, 0.25, \dots, 0.95$. Fig. 4 shows $D_A(z)$ for our fiducial model, along with the predicted error on D_A . The green dashed lines show the change in D_A when h changes by 0.01. The lower panel shows the residual from the fiducial angular diameter distance.

We consider the cosmological constraints that could be derived from such a data set. To do so, we generate an artificial data vector comprised of the fiducial angular diameter distance and the errors from fig. 4, and fit for the cosmological parameters h and Ω_m assuming a flat Λ CDM model. The results are shown as the blue contours in fig. 5. We find $\sigma_h \approx 0.009$, corresponding to a 1.3% measurement of h . The uncertainty in the recovered matter density parameters is large: $\sigma_{\Omega_m} \approx 0.042$. This can be compared to the constraint derived from the combined Pantheon supernova sample from Scolnic et al. (2018), shown in fig. 5 as a green band ($\Omega_m = 0.298 \pm 0.022$). Adding the Pantheon data set as an external prior, our constraint on the Hubble parameter improves to $\sigma_h \approx 0.005$, or 0.7%. This is shown as the red contours in fig. 5.

The large uncertainty in the recovered matter density parameter in our analysis demonstrates that the sensitivity of the proposed measurement to matter density and dark energy is quite limited: this measurement is simply not competitive with supernova measurements. This could in principle change if the cluster density is increased, and provided all shape parameters can be calibrated from simulations, but our analysis suggests such prospects are dim. Indeed, assuming all known nuisance parameters that can be calibrated from simulation are perfectly known, the error in w_0 for flat w CDM cosmology is $\sigma_w = 0.26$. By contrast, the predicted uncertainty in the Hubble parameter is exciting, and provides strong evidence that implementing the proposed measurement in the DESI data set, particularly within the context of the Bright Galaxy Survey, may result in highly competitive measurements of the Hubble constant. We emphasise that these constraints would be enabled by the relation between cluster size and galaxy velocity dispersion as calibrated from numerical simulations. As such, this standard-ruler measurement is calibrated exclusively through our understanding of gravity. While baryonic physics could in principle impact these predictions, the fact that the cluster radii are large suggests that baryonic effects on R_{edge} will be small, though this will need to be quantitatively characterised in simulations. Given these features, our measurement is much more akin to a sound-horizon based measurement than the supernova measurements. That is to say, our calibration would ultimately be based on well understood physical processes, specifically, gravity.

5 CONCLUSIONS

We have presented a novel method for measuring cosmological distances using the spatial extent of orbiting galaxies in halos as a standard ruler. Conceptually, a measurement of the galaxy velocity dispersion allows us to infer a halo's size. This size can in turn be detected as a specific angular scale, thereby enabling a measurement of the distance to the galaxy cluster. Critically, this is a first-principles physics-based calibration, and therefore does not rely on distance ladder measurements. At the same time, it shares no theoretical systematics with baryon acoustic oscillation and CMB measurements.

To determine whether this measurement is interesting in principle, we adopted a fiducial model for the calibration between velocity dispersion and size, and proceeded to measure the Hubble constant, using spectroscopic galaxies from SDSS DR14 and photometrically-selected galaxy clusters from the SDSS redMaPPer algorithm. We emphasise that since we have *assumed* the scaling relation between cluster velocity dispersion and halo radii, the central value of our Hubble constant measurement is meaningless. Our goal is only to forecast the precision of this newly proposed measurement. Our baseline uncertainty in the dimensionless Hubble constant as measured in the SDSS is $\sigma_h \approx 0.021$ (3%). Unsurprisingly, this precision is degraded if the calibration of the cluster edge radius in eqn. (3) is uncertain. Conversely, if all halo structure parameters are held fixed, the recovered uncertainty in the Hubble constant in the SDSS is $\sigma_h = 0.0088$ (1.2%).

We also performed a forecast of the constraining power of our method when using DESI data. We assumed a cluster catalogue extending to $z = 1$, where the cluster density was estimated using the DES Y1 redMaPPer cluster sample. Adopting a flat Λ CDM cosmology, we recover a 1.3% of the Hubble constant, which is dominated by low-redshift distance measurements. As we noted earlier, assuming that the redMaPPer catalogue could be extended to redshift $z = 1$ across the full DESI footprint is likely over-optimistic. Even with this assumption, however, we find that the corresponding error on the matter density is large: our proposed method is not competitive as a probe of dark energy. Thus, our proposed measurement works best as a low redshift technique for precisely measuring the Hubble constant. When we include a prior of $\Omega_m = 0.298 \pm 0.022$ from the combined Pantheon supernova analysis of Scolnic et al. (2018), our constraints improve to a 0.7% uncertainty on the Hubble constant. This level of precision more than suffices for unambiguously distinguishing between local and CMB-based values of the Hubble constant at high confidence.

There are, of course, additional obstacles that will need to be resolved in order to enable the proposed measurement, most notably characterising the impact of cluster selection effects on the recovered Hubble parameter. While such systematics may well increase the final delivered error substantially, there also exists the possibility of significant improvements relative to our forecast, particularly by calibrating additional halo structural parameters, e.g. the galaxy density profiles and the in-fall velocity dispersion profiles. Overall, our results provide strong motivation for aggressively pursuing the calibration and systematics tests necessary to enable the proposed Hubble constant measurement. If successful, such a program could provide smoking gun evidence either in favour or against the current Hubble tension problem.

ACKNOWLEDGEMENTS

ELW and ER are supported by the DOE grant DE-SC0015975. ER is also supported by DOE grant DE-SC0009913, and by NSF grant

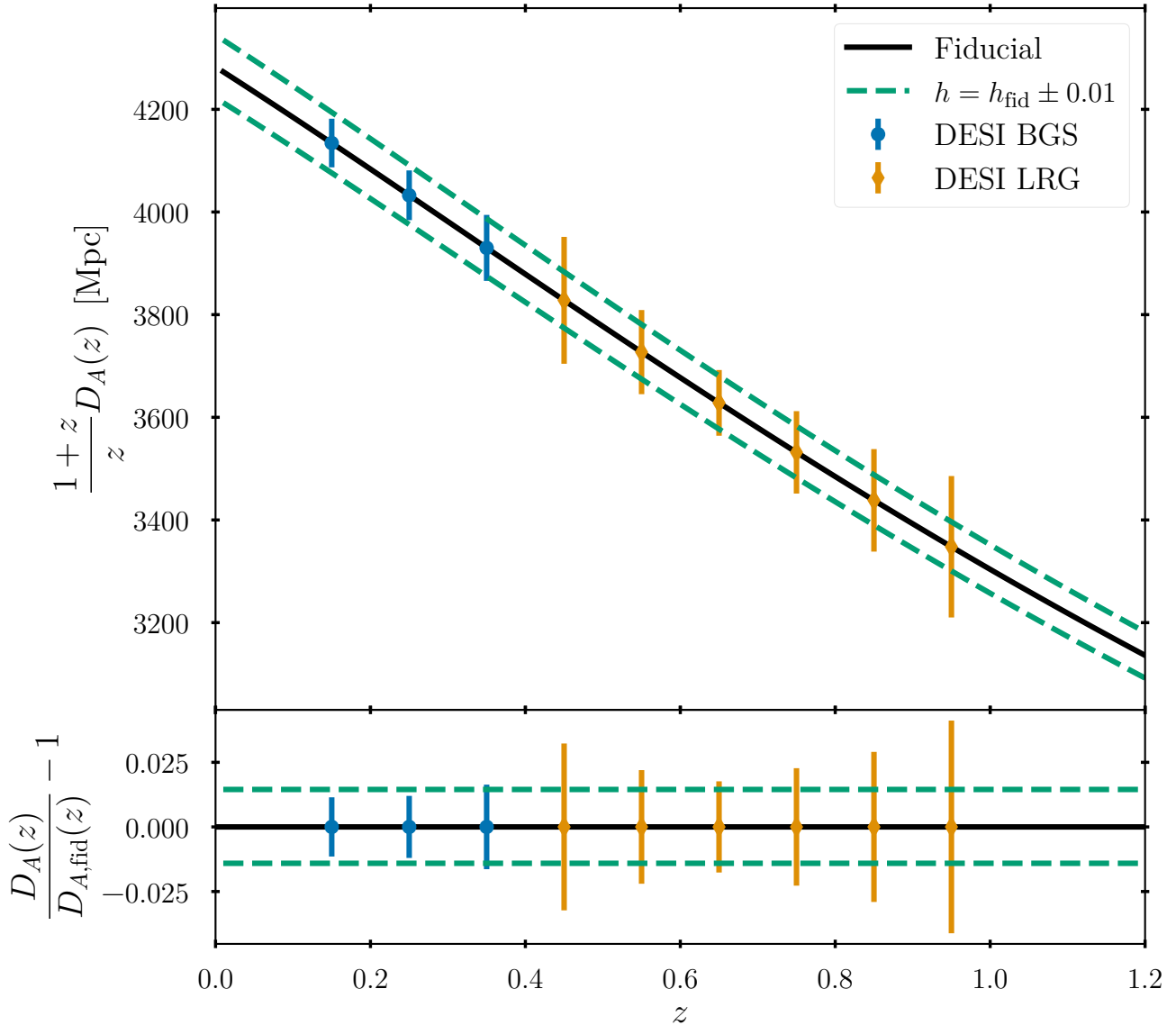


Figure 4. Forecast of the error on the estimated angular diameter distance for DESI. The solid black line is the angular diameter distance for our fiducial cosmology. The dashed green lines are the angular diameter distance when the dimensionless Hubble constant is changed by 0.01 relative to the fiducial value. The blue error bars show the predicted uncertainty on the fiducial cosmology that can be measured by the DESI BGS sample assuming perfect calibration, and the orange error bars show the same but for the DESI LRG sample. The bottom panel shows the residual in the angular diameter distance relative to the fiducial cosmology.

2009401. HA and DN acknowledge support from Yale University. ER and DN also acknowledges funding from the Cottrell Scholar program of the Research Corporation for Science Advancement.

Funding for SDSS-III has been provided by the Alfred P. Sloan Foundation, the Participating Institutions, the National Science Foundation, and the U.S. Department of Energy Office of Science. The SDSS-III web site is <http://www.sdss3.org/>.

SDSS-III is managed by the Astrophysical Research Consortium for the Participating Institutions of the SDSS-III Collaboration including the University of Arizona, the Brazilian Participation Group, Brookhaven National Laboratory, Carnegie Mellon University, University of Florida, the French Participation Group, the German Participation Group, Harvard University, the Instituto de Astrofísica de

Canarias, the Michigan State/Notre Dame/JINA Participation Group, Johns Hopkins University, Lawrence Berkeley National Laboratory, Max Planck Institute for Astrophysics, Max Planck Institute for Extraterrestrial Physics, New Mexico State University, New York University, Ohio State University, Pennsylvania State University, University of Portsmouth, Princeton University, the Spanish Participation Group, University of Tokyo, University of Utah, Vanderbilt University, University of Virginia, University of Washington, and Yale University.

Funding for the Sloan Digital Sky Survey IV has been provided by the Alfred P. Sloan Foundation, the U.S. Department of Energy Office of Science, and the Participating Institutions. SDSS-IV acknowledges support and resources from the Center for High-

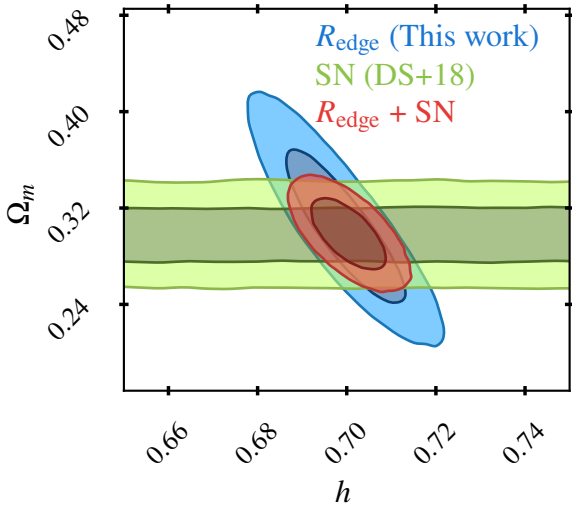


Figure 5. Contours resulting from a 2-parameter (h and Ω_m) fit to the Hubble diagram data in fig. 4. The blue contours are the result of fitting to the “data” given by the blue and orange points in fig. 4. The green contours are the result of fitting the same parameters to the pantheon supernova sample (Scolnic et al. 2018). The red contours are the result of a combined analysis including both supernova data as well as the angular diameter distance “data” from fig. 4.

Performance Computing at the University of Utah. The SDSS web site is www.sdss.org.

SDSS-IV is managed by the Astrophysical Research Consortium for the Participating Institutions of the SDSS Collaboration including the Brazilian Participation Group, the Carnegie Institution for Science, Carnegie Mellon University, the Chilean Participation Group, the French Participation Group, Harvard-Smithsonian Center for Astrophysics, Instituto de Astrofísica de Canarias, The Johns Hopkins University, Kavli Institute for the Physics and Mathematics of the Universe (IPMU) / University of Tokyo, the Korean Participation Group, Lawrence Berkeley National Laboratory, Leibniz Institut für Astrophysik Potsdam (AIP), Max-Planck-Institut für Astronomie (MPIA Heidelberg), Max-Planck-Institut für Astrophysik (MPA Garching), Max-Planck-Institut für Extraterrestrische Physik (MPE), National Astronomical Observatories of China, New Mexico State University, New York University, University of Notre Dame, Observatório Nacional / MCTI, The Ohio State University, Pennsylvania State University, Shanghai Astronomical Observatory, United Kingdom Participation Group, Universidad Nacional Autónoma de México, University of Arizona, University of Colorado Boulder, University of Oxford, University of Portsmouth, University of Utah, University of Virginia, University of Washington, University of Wisconsin, Vanderbilt University, and Yale University.

Funding for the DES Projects has been provided by the U.S. Department of Energy, the U.S. National Science Foundation, the Ministry of Science and Education of Spain, the Science and Technology Facilities Council of the United Kingdom, the Higher Education Funding Council for England, the National Center for Supercomputing Applications at the University of Illinois at Urbana-Champaign, the Kavli Institute of Cosmological Physics at the University of Chicago, the Center for Cosmology and Astro-Particle Physics at the Ohio State University, the Mitchell Institute for Fundamental Physics and Astronomy at Texas A&M University, Financiadora de

Estudos e Projetos, Fundação Carlos Chagas Filho de Amparo à Pesquisa do Estado do Rio de Janeiro, Conselho Nacional de Desenvolvimento Científico e Tecnológico and the Ministério da Ciência, Tecnologia e Inovação, the Deutsche Forschungsgemeinschaft and the Collaborating Institutions in the Dark Energy Survey.

The Collaborating Institutions are Argonne National Laboratory, the University of California at Santa Cruz, the University of Cambridge, Centro de Investigaciones Energéticas, Medioambientales y Tecnológicas-Madrid, the University of Chicago, University College London, the DES-Brazil Consortium, the University of Edinburgh, the Eidgenössische Technische Hochschule (ETH) Zürich, Fermi National Accelerator Laboratory, the University of Illinois at Urbana-Champaign, the Institut de Ciències de l’Espai (IEEC/CSIC), the Institut de Física d’Altes Energies, Lawrence Berkeley National Laboratory, the Ludwig-Maximilians Universität München and the associated Excellence Cluster Universe, the University of Michigan, NFS’s NOIRLab, the University of Nottingham, The Ohio State University, the University of Pennsylvania, the University of Portsmouth, SLAC National Accelerator Laboratory, Stanford University, the University of Sussex, Texas A&M University, and the OzDES Membership Consortium.

Based in part on observations at Cerro Tololo Inter-American Observatory at NSF’s NOIRLab (NOIRLab Prop. ID 2012B-0001; PI: J. Frieman), which is managed by the Association of Universities for Research in Astronomy (AURA) under a cooperative agreement with the National Science Foundation.

The DES data management system is supported by the National Science Foundation under Grant Numbers AST-1138766 and AST-1536171. The DES participants from Spanish institutions are partially supported by MICINN under grants ESP2017-89838, PGC2018-094773, PGC2018-102021, SEV-2016-0588, SEV-2016-0597, and MDM-2015-0509, some of which include ERDF funds from the European Union. IFAE is partially funded by the CERCA program of the Generalitat de Catalunya. Research leading to these results has received funding from the European Research Council under the European Union’s Seventh Framework Program (FP7/2007-2013) including ERC grant agreements 240672, 291329, and 306478. We acknowledge support from the Brazilian Instituto Nacional de Ciência e Tecnologia (INCT) e-Universe (CNPq grant 465376/2014-2).

This manuscript has been authored by Fermi Research Alliance, LLC under Contract No. DE-AC02-07CH11359 with the U.S. Department of Energy, Office of Science, Office of High Energy Physics.

This research made use of Python, SciPy (Virtanen et al. 2020), NumPy (van der Walt et al. 2011), IPython (Perez & Granger 2007), Matplotlib (Hunter 2007), and ChainConsumer (Hinton 2016). This research also made use of Astropy,² a community-developed core Python package for Astronomy (Astropy Collaboration et al. 2013, 2018).

DATA AVAILABILITY

The spectroscopic data underlying this article are available via query through the SDSS query service CasJobs at <http://skyserver.sdss.org/CasJobs/>. The SDSS redMaPPer cluster catalogue is available at <http://risa.stanford.edu/redmapper>. The DES Y1 redMaPPer catalogue is available for download at <https://des.ncsa.illinois.edu/releases/y1a1/key-catalogs/key-redmapper>.

² <http://www.astropy.org>

REFERENCES

- Abolfathi B., et al., 2018, *ApJS*, 235, 42
- Adhikari S., Dalal N., Chamberlain R. T., 2014, *J. Cosmology Astropart. Phys.*, 2014, 019
- Aihara H., et al., 2011a, *ApJS*, 193, 29
- Aihara H., et al., 2011b, *ApJS*, 195, 26
- Astropy Collaboration et al., 2013, *A&A*, 558, A33
- Astropy Collaboration et al., 2018, *AJ*, 156, 123
- Aung H., Nagai D., Rozo E., Garcia R., 2020, arXiv e-prints, p. [arXiv:2003.11557](https://arxiv.org/abs/2003.11557)
- Bertschinger E., 1985, *ApJS*, 58, 39
- Birrer S., et al., 2020, arXiv e-prints, p. [arXiv:2007.02941](https://arxiv.org/abs/2007.02941)
- Blanton M. R., et al., 2017, *AJ*, 154, 28
- Busch P., White S. D. M., 2017, *MNRAS*, 470, 4767
- Chang C., et al., 2018, *ApJ*, 864, 83
- Contigiani O., Hoekstra H., Bahé Y. M., 2019, *MNRAS*, 485, 408
- DESI Collaboration et al., 2016, arXiv e-prints, p. [arXiv:1611.00036](https://arxiv.org/abs/1611.00036)
- Di Valentino E., et al., 2020, arXiv e-prints, p. [arXiv:2008.11284](https://arxiv.org/abs/2008.11284)
- Diemer B., 2020, arXiv e-prints, p. [arXiv:2007.10992](https://arxiv.org/abs/2007.10992)
- Eisenstein D. J., et al., 2011, *AJ*, 142, 72
- Foreman-Mackey D., Hogg D. W., Lang D., Goodman J., 2013, *PASP*, 125, 306
- Freedman W. L., et al., 2020, *ApJ*, 891, 57
- Gómez-Valent A., Amendola L., 2019, arXiv e-prints, p. [arXiv:1905.04052](https://arxiv.org/abs/1905.04052)
- Haridasu B. S., Luković V. V., Moresco M., Vittorio N., 2018, *J. Cosmology Astropart. Phys.*, 2018, 015
- Hinton S. R., 2016, *The Journal of Open Source Software*, 1, 00045
- Hunter J. D., 2007, *Computing in Science and Engineering*, 9, 90
- Ilbert O., et al., 2009, *ApJ*, 690, 1236
- Khetan N., et al., 2020, arXiv e-prints, p. [arXiv:2008.07754](https://arxiv.org/abs/2008.07754)
- Knox L., Millea M., 2020, *Phys. Rev. D*, 101, 043533
- Kochanek C. S., 2020, *MNRAS*, 493, 1725
- McClintock T., et al., 2019, *MNRAS*, 482, 1352
- More S., Diemer B., Kravtsov A. V., 2015, *ApJ*, 810, 36
- More S., et al., 2016, *ApJ*, 825, 39
- Murata R., Sunayama T., Oguri M., More S., Nishizawa A. J., Nishimichi T., Osato K., 2020, *PASJ*, 72, 64
- Perez F., Granger B. E., 2007, *Computing in Science and Engineering*, 9, 21
- Pesce D. W., et al., 2020, *ApJ*, 891, L1
- Planck Collaboration et al., 2018, arXiv e-prints, p. [arXiv:1807.06209](https://arxiv.org/abs/1807.06209)
- Riess A. G., Casertano S., Yuan W., Macri L. M., Scolnic D., 2019, *ApJ*, 876, 85
- Roza E., Rykoff E. S., Becker M., Reddick R. M., Wechsler R. H., 2015, *MNRAS*, 453, 38
- Rykoff E. S., et al., 2014, *ApJ*, 785, 104
- Scolnic D. M., et al., 2018, *ApJ*, 859, 101
- Shin T., et al., 2019, *MNRAS*, 487, 2900
- Sunayama T., More S., 2019, *MNRAS*, 490, 4945
- The LIGO Scientific Collaboration the Virgo Collaboration 2019, arXiv e-prints, p. [arXiv:1908.06060](https://arxiv.org/abs/1908.06060)
- Tomooka P., Roza E., Wagoner E. L., Aung H., Nagai D., Safonova S., 2020, arXiv e-prints, p. [arXiv:2003.11555](https://arxiv.org/abs/2003.11555)
- Umetsu K., Diemer B., 2017, *ApJ*, 836, 231
- Verde L., Treu T., Riess A. G., 2019, *Nature Astronomy*, 3, 891
- Virtanen P., et al., 2020, *Nature Methods*, 17, 261
- Wong K. C., et al., 2020, *MNRAS*,
- Zürcher D., More S., 2019, *ApJ*, 874, 184
- van der Walt S., Colbert S. C., Varoquaux G., 2011, *Computing in Science and Engineering*, 13, 22

This paper has been typeset from a $\text{\TeX}/\text{\LaTeX}$ file prepared by the author.